(NASA-CR-162829) THE EFFECT OF TEST SYSTEM MISALIGNMENT IN THE DYNAMIC TENSION TEST (Iowa Univ.) 44 p HC A03/MF A01 CSCL 20K

N80-19564

Unclas

G3/39 47392

Division of Materials Engineering

COLLEGE OF ENGINEERING

THE UNIVERSITY OF IOWA

Iowa City, Iowa 52242

THE EFFECT OF TEST SYSTEM MISALIGNMENT IN THE DYNAMIC TENSION TEST

by

Han C. Wu, T. P. Wang, and M. C. Yip
Division of Materials Engineering
The University of Iowa
Iowa City, Iowa 52242

Report G302-80-001

Prepared for
NASA-Langley Research Center
Hampton, Virginia

Grant No. NSG 1499

March 1, 1980

ABSTRACT

An analysis of test system misalignment is presented for dynamic tension test. Sheet type rectangular 1100-0 aluminum specimens are used for discussion.

For a constant strain rate tension test, the strain rate is constant only on the neutral axis of the specimen. The following results have been obtained: (a) The lower the strain rate is, the more significant the misalignment errors become. (b) Misalignment errors of 50% have been found at the extreme fibers of the specimen. (c) The strain rate variation in the cross-section decreases with increasing plastic strain and vanishes at plastic strain equal to 0.8% at the midspan of the specimen. (d) The neutral axis will shift toward the centerline of the specimen as the plastic strain increases. But, it will reach a limit and will not completely move back to the centerline.

A more restricted uniform strain rate formulation is also presented. The result is compared with that of the nonuniform strain rate formulation.

1. INTRODUCTION

The effect of misalignment in a tensile test system has been previously investigated by a number of investigators [1,2]. These investigators have also identified the sources of misalignment as poor conformance of specimen centerline to top and bottom grip centerlines, poor alignment of the top and bottom grip centerlines, and inaccurate machining of the test specimen itself. A more detailed description of test system misalignment and the discussion concerning the need for such investigation may be found in Refs. [1,2] and also in Wu and Rummler [3].

In [3], a comprehensive analysis of misalignment effect was presented for tension test under static loading condition. In the analysis, three cases of misalignment were considered, which were the symmetric case, the cantilever case, and the case of the pinned specimen with eccentricity. It was found that the symmetric case is the most critical one as far as the effect of misalignment is concerned. In addition, Wu and Rummler concluded that the stress-strain curve is significantly affected by misalignment at strain levels corresponding to the knee portion of the stress-strain curve. Moreover, the strain at the outermost fibers of the specimen is strongly affected by misalignment and the misalignment effects are smaller for load trains with longer pull rods.

The dynamic mechanical properties of materials have become increasingly important in the recent years. Tension tests have been conducted at various fixed strain rates to determine the dynamic behavior of materials. The problem of test system alignment which exists in the static test would also carry over to the dynamic test. However, to the present investigators' knowledge, the alignment problem under dynamic tensile load has not been investigated in the literature.

In this paper, an analysis of test system misalignment is presented for dynamic tension test. For simplicity, rectangular specimens of the sheet type are considered in this investigation. Only the symmetric case of misalignment is studied due to the finding of [3] that this is the most severe case. Specimens of 1100-0 aluminum have been chosen for investigation. The reason for using this material as an example for discussion is that the constitutive equation employed in the present analysis has been shown to describe both the dynamic stress-strain behavior and creep* for this material [4] and the material constants have already been determined. Theoretically speaking, the method presented herein would also apply to other materials.

The purpose of this study is to investigate the effect of strain rate on the misalignment problem. The equations derived are used to calculate the strain rate distribution and the misalignment error at the center section of the specimen. The center section is of interest, since the strain measuring devices (extensometer, strain gage, etc.) are usually attached to the center of the specimen.

In Section 2, the constitutive equation used in the analysis is briefly described. The field equations for the misalignment problem found in the dynamic tension test and their discretized numerical models are formulated in Section 3. In the formulation, the strain rates are nonuniform across a cross-section of the specimen although the specimen is subjected to a constant strain rate test (constant strain rate at the neutral axis (N.A.)). A more restricted formulation where strain rate is constant all over the specimen is included in Appendix A. The results of this uniform strain rate formulation

*The ultimate goal of this research progam is to determine the effect of misalignment in the creep test. The results obtained in this report will be used directly in the creep investigation.

serve as the initial guess for obtaining numerical solutions of the highly nonlinear equations of Section 3. A detailed computing procedure for solution of this set of nonlinear equations is described in Appendix B.

The numerical results and discussion are presented in Section 4. It is believed that the effort made in this research contributes toward a more thorough understanding of the misalignment effect in the tension test.

2. THE CONSITUTIVE EQUATION

The constitutive equation used in this investigation is the same as that given by Wu and Yip [5] for strain rate sensitive materials. This is a modified version of the endochronic constitutive equation originally proposed by Valanis [6]. For constant strain rate monotonic tension test, the constitutive equation is

$$\sigma = \frac{1}{k}(1 + \beta\zeta)\left[\sigma_0 - (\sigma_0 - \sigma_y)(1 + \beta\zeta)^{-n}\right] \tag{1}$$

in which σ is the stress; σ_0 is the intercept of the asymptotic line of the reference stress-strain curve with the stress axis; σ_y is the yield stress; β and n are material constants; z is the intrinsic time defined by

$$\zeta = k(\dot{\theta})\theta \tag{2}$$

and k is the strain rate sensitivity function governed by

$$k(\dot{\theta}) = 1 - \beta_s \ln\left(\frac{\dot{\theta}}{\dot{\theta}_R}\right) \tag{3}$$

where

$$\theta = \varepsilon - \sigma/E \tag{4}$$

is the plastic strain, ε is the total strain, E is Young's modulus, β_s is a material constant, and $\dot{\theta}_R$ is a reference strain rate.

Equation (1) represents a set of constant $\dot{\theta}$ stress-strain curves. For 1100-0 aluminum at 150°C, the function $k(\dot{\theta})$ was determined by Wu and Chen [4] from a set of experimental data for the strain rate range of 10^{-4} to 10^{3} sec^{-1}. This function is reproduced in Fig. 1, where β_s and $\dot{\theta}_R$ are equal to

3.643×10^{-2} and 1.30×10^{-5} sec^{-1}, respectively. Figure 2 shows three σ vs. θ curves, each corresponding to a constant $\dot{\theta}$ with corresponding k values equal to 1.00, 0.75 and 0.60. These three curves are used in the study of misalignment to be reported in the next section.

Finally, it must be mentioned that equation (1) describes only the plastic behavior of the material under consideration.

3. FORMULATION OF THE MISALIGNMENT PROBLEM

When a misaligned specimen undergoes a constant strain rate dynamic tensile test, it is expected that the strain rate varies both along the lateral and the longitudinal directions of the specimen. The strain rate remains constant only along the N.A. which is defined as the location of the mean stress (load/area) as in Ref. [3].

Specimen dimensions and the coordinate system are chosen the same way as in Ref. [3], and the latter is shown in Fig. 3(a). Figure 3(b) shows the load train configuration of the symmetric case of misalignment. In the analysis, it is assumed that plane cross-sections remain plane during deformation. Thus, the strain ε at a point in the specimen is given by

$$\varepsilon(x,y) = \bar{\varepsilon} - \frac{y}{\rho(x)} \tag{5}$$

where x and y are coordinates shown in Fig. 3(a), $\bar{\varepsilon}$ is the strain on N.A., and $\rho(x)$ is the radius of curvature of the specimen. The radius of curvature is expressed in terms of the strains of the top fiber ε_T and the bottom fiber ε_B through the expression

$$\rho(z) = \frac{h}{\varepsilon_B - \varepsilon_T} \tag{6}$$

in which h is the width of the specimen. The distance d(x), which specifies the location of the N.A. and is measured from the bottom fiber of the specimen is given by

$$\frac{d(x)}{h} = \frac{\varepsilon_B - \bar{\varepsilon}}{\varepsilon_B - \varepsilon_T} \tag{7}$$

Due to the variation of strain rate in the specimen, the misalignment problem is quite complicated mathematically. Only numerical solutions are feasible. Therefore, the specimen is discretized as shown in Fig. 4. The stress, the strain, and the strain rate in each element are assumed to have constant values. Only half of the specimen needs to be considered due to the symmetric loading condition. Thus, the half span is cut into I sections along the longitudinal direction and resulted in I + 1 planes to be investigated (see Fig. 4a). The lateral direction (the width h) is cut into J sections as shown in Fig. 4b.

Based on the discrete model and the constitutive equation (1), the stress-strain relation in the element (i,j) is

$$\sigma_{ij} = \frac{1}{k_{ij}} (1 + \beta\zeta_{ij}) \left[\sigma_0 - (\sigma_0 - \sigma_y)(1 + \beta\zeta_{ij})^{-n}\right] \quad ;$$

$$\text{with } i = 1,\ldots,I+1 \quad ; \qquad j = 1,\ldots,J \tag{8}$$

While equation (1) is exact, an additional assumption is made to arrive at equation (8). It is assumed that a generic point in the specimen maintains the same strain rate throughout the test although the strain rate may vary from point to point in a cross-section. Since the strain rate at a generic point varies only very slightly (this is justified by the numerical results), this assumption constitutes a close approximation when equation (8) is used to compute the stress.

The strain rate sensitivity function is

$$k_{ij} = 1 - \beta_s \ln \left(\frac{\dot{\theta}_{ij}}{\dot{\theta}_R}\right) \tag{9}$$

Since the reference plastic strain rate $\dot{\theta}_R$ may be different than the strain rate at the N.A., $\dot{\bar{\theta}}$, it is convenient to rewrite equation (9) as

$$k_{ij} = 1 - \beta_s \ln \left(\frac{\dot{\theta}_{ij}}{\dot{\bar{\theta}}}\right) - \beta_s \ln \left(\frac{\dot{\bar{\theta}}}{\dot{\theta}_R}\right) \tag{10}$$

It is remarked that $\dot{\bar{\theta}}$ is prescribed for each test and $\dot{\theta}_R$ is known from the experimental data (see Ref. [4]). Hence the last term on the right-hand side of equation (10) is determined. The strain rate sensitivity function on the N.A., denoted by $\bar{k}$, may be obtained by putting $\dot{\theta}_{ij} = \dot{\bar{\theta}}$ in equation (10). Thus,

$$\bar{k} = 1 - \beta_s \ln \left(\frac{\dot{\bar{\theta}}}{\dot{\theta}_R}\right) \tag{11}$$

and equation (10) reduces to

$$k_{ij} = \bar{k} - \beta_s \ln \left(\frac{\dot{\theta}_{ij}}{\dot{\bar{\theta}}}\right) \tag{12}$$

In the numerical computation, the strain rates are expressed by the increments, i.e.,

$$k_{ij} = \bar{k} - \beta_s \ln \left(\frac{\Delta\theta_{ij}}{\Delta\bar{\theta}}\right) \tag{13}$$

Furthermore, from equations (4) and (2), it is obtained

$$\sigma_{ij} = \epsilon_{ij} - \sigma_{ij}/E \tag{14}$$

and

$$\zeta_{ij} = k_{ij} (\epsilon_{ij} - \sigma_{ij}/E) \tag{15}$$

The linear distribution of strain in a cross-section renders

$$\varepsilon_{ij} = \varepsilon_{iT} + (\varepsilon_{iB} - \varepsilon_{iT}) \left(\frac{2j - 1}{J}\right) \; ; \qquad j = 1,\ldots,J \tag{16}$$

for the strain at the ith plane (see Fig. 4b). The strains ε_{iT} and ε_{iB} are referred to the continuous, deformed cross-section, whereas ε_{ij} is assigned to the discretized planes of the numerical model.

Balance of force acting on the specimen gives

$$P = \int_A \sigma \, dA = b \int \sigma \, dy \tag{17}$$

in which P is the force, b is the thickness and A is the cross-sectional area of the specimen. In a discrete form, this equation leads to

$$P = \frac{bh}{J} \sum_j \sigma_{ij} \; ; \qquad i = 1,\ldots,I + 1 \tag{18}$$

for the ith plane. The expression h/J is the width of the element under consideration at the ith section.

The stress $\bar{\sigma}$ and the intrinsic time $\bar{\zeta}$ at the N.A. are related to the load P by

$$\frac{P}{A} = \bar{\sigma} = \frac{1}{\bar{k}} (1 + \beta\bar{\zeta}) \; [\sigma_0 - (\sigma_0 - \sigma_y)(1 + \beta\bar{\zeta})^{-n}] \tag{19}$$

Note that the quantities $\bar{\zeta}$, $\bar{k}$, and $\bar{\sigma}$ are assigned as input during numerical calculation.

The balance of moment is given by

$$M(x) = - \int_A \sigma y \, dA = - \rho\bar{\varepsilon}P + b\rho \int \sigma\varepsilon \, dy \tag{20}$$

In the discrete model, this equation becomes

$$M_i = -\rho_i \bar{\varepsilon} P + \frac{bh}{J} \rho_i \sum_{j=1}^{J} \sigma_{ij} \varepsilon_{ij} \quad ; \quad i = 1,\ldots,I+1 \tag{21}$$

for the ith plane.

Referring to Fig. 3(b), the following equation is obtained

$$M_i = P \left(\delta^* + u_i - L \frac{du_{I+1}}{dx} \right) \tag{22}$$

where

$$\delta^* = \delta + (d_s - h/2) \tag{23}$$

and u_i is the deflection at ith section, δ is the eccentricity, L is the pull rod length, and d_s denotes the location of the N.A. at the grip end. The distance d_s is that of d evaluated at $i = I + 1$ and is further given by

$$d_s = h \frac{\varepsilon_{I+1,B} - \bar{\varepsilon}}{\varepsilon_{I+1,B} - \varepsilon_{I+1,T}} \tag{24}$$

where $\varepsilon_{I+1,T}$ and $\varepsilon_{I+1,B}$ are strains of top and bottom fibers respectively at the grip end.

The curvature relation is

$$\frac{1}{\rho_i} = \frac{d^2 u_i}{dx_i^2} \tag{25}$$

which in its difference form is

$$\frac{\varepsilon_{iB} - \varepsilon_{iT}}{h} = \frac{u_{i+1} - 2u_i + u_{i-1}}{\Delta x^2} \quad ; \quad i = 1,\ldots,I-1 \tag{26}$$

where Δx is the uniform distance between cross-sectional planes.

The formulation of the misalignment problem under dynamic loading condition is now complete. The set of equations (8), (15), (18), (21), (24) and (26) constitutes a system of highly nonlinear equations, which can be solved numerically for variables σ_{ij}, ε_{iT}, ε_{iB}, ζ_{ij}, u_i and d_s for a specified load P subjected to the following boundary conditions:

$$\frac{du}{dx} = 0 \qquad \text{at} \qquad x = 0 \tag{27}$$

and

$$u = 0 \qquad \text{at} \qquad x = \ell/2 \tag{28}$$

In the above equation, ℓ is the length of the specimen.

4. RESULTS AND DISCUSSION

During analyses, three different values of strain rate are assigned to the N.A. as input data to investigate the influence of strain rate on misaligned tensile specimen. The strain rates investigated are 1.30×10^{-5}, 1.24×10^{-2}, and 7.63×10^{-1} sec^{-1} and their corresponding values of strain rate sensitivity function k are 1.00, 0.75 and 0.60.

The sheet type rectangular speciments are used. The geometrical data for the specimen are

pull rod length/specimen length = 2

specimen length (ℓ) = 63.5 mm

specimen width (h) = 12.7 mm

specimen thickness (b) = 3.2 mm

eccentricity δ = 0.05 h

In order to reduce computer time, only four sections have been cut along both the longitudinal and the lateral directions of the specimen, i.e., I = 4 and J = 4. Thus, the unknown variables have been reduced to 55 in number and the set of nonlinear equations discussed in Section 3 consists now of 55 equations. Due to the minimum number of elements in the discrete numerical model, some unstable numberical results are experienced at the grip end at the larger strain level and will be discussed later in the text. Nevertheless, this model provides a consistent output under a variety of loading conditions. Since the area of interest for the misalignment analysis lies in the midspan of the specimen (the measuring devices are usually attached to the midspan), most of the results to be discussed are related to this area.

The normalized strain rate sensitivity function $k/\bar{k}$ for the top and bottom fibers at the midspan is plotted in Fig. 5 against the plastic strain $\bar{\theta}$ for the three strain rate levels previously mentioned. It is seen that k decreases (increases) rapidly at small strain level for top (bottom) fiber until $\bar{\theta}$ reaches 0.8%, when k becomes uniform across the cross-section. Hence, the variation of strain rate in a cross-section diminishes as strain increases. This phenomenon can be explained from the following equation

$$\Delta\theta_{ij} = \Delta\bar{\theta}\, e^{\frac{\bar{k}}{\beta_s}\left(1 - \frac{k_{ij}}{\bar{k}}\right)} \tag{29}$$

which is obtained by rearranging equation (13). At the small plastic strain range, $k/\bar{k}$ is greater (smaller) than unity for the top (bottom) fibers, and θ_{ij} increases slower (faster) than $\bar{\theta}$ and causes misalignment errors. As $\bar{\theta}$ exceeds 0.8%, $k/\bar{k}$ approaches to unity and equation (29) leads to

$$\Delta\theta_{ij} \approx \Delta\bar{\theta} \tag{30}$$

The implication of equation (30) is that, at larger strain level, the relative error arisen from misalignment is always decreasing.

The effect of strain rate can be further examined from Fig. 6, where k at the misdpan is shown varying with the width of the specimen for two levels of $\bar{\theta}$. It can be concluded that the range of variation of k at a cross-section is wider and that a uniform distribution of strain rate is achieved at a larger strain level for larger strain rate loading.

The misalignment error at the geometrical centerline (or center error) at the midspan is shown in Fig. 7* for three levels of strain rate. The center error, denoted by $E_c(\%)$, is defined by $(\varepsilon_c - \bar{\varepsilon})/\bar{\varepsilon}$. It is seen that the center error is always decreasing in the plastic range and vanishes at large strain. This result is also expected from equation (29). Generally, the center error is within 2% for annealed aluminum undergoing plastic deformation and vanishes mostly when the plastic strain is 2% or more. Although this investigation does not cover the effect of misalignment in the elastic range, it is expected that a result similar to that of Ref. [3] prevails, i.e., the misalignment effect is very significant near the interface between the elastic and plastic ranges, or the knee portion of the stress-strain curve. The error would then decrease as the plastic strain increases.

The most important finding from Fig. 7 is that the misalignment effect reduces with increasing strain rate. An interpretation of this finding is that the material exhibits higher resistance to deformation at higher strain rate and this help retard the influence of misalignment.

Misalignment errors of the top (E_T) and bottom (E_B) fibers are plotted in Fig. 8. They have the same trend as the center error but with much greater magnitudes. The errors at lowest strain rate considered ($\bar{k} = 1$) and at $\bar{\theta} = 0.1\%$ are +50% and -45% for bottom and top fibers, respectively. Therefore, any investigation which is related to the local deformation of the extreme fibers at small plastic strain range may lead to invalid conclusion due to the significant misalignment errors discussed above.

*Due to the limitation of computational funds, the curves for $\bar{k} = 0.75$ and 0.60 have not been completed at higher $\bar{\theta}$ level. However, it is expected that the curves will follow the trend shown by the dashed lines in Figs. 7-10.

The location of the N.A. is plotted in Fig. 9 for the midspan. It is seen that the smaller the strain rate is, the greater mobility the N.A. has. The peak values of d/h is resided within the range of $\bar{\theta}$ equal to 0.5% to 1.0% for the three strain rates considered and can be approximately correlated to the points on the stress-strain curves where the stress-strain curves begin to flatten out. These points are shown by arrows in Fig. 2.

It is known from the discussion earlier that $k/\bar{k} \to 1$ when $\bar{\theta} \geq 0.8\%$. Under this condition equation (30) leads to

$$\theta_{ij} - \bar{\theta} = C_{ij} \qquad \text{for } \frac{k}{\bar{k}} \to 1 \tag{31}$$

where C_{ij} is a constant which varies along the cross-section. As the deformation continues to the extent that the plastic strain dominates the total strain, the expression for the location of the N.A. can then be obtained from equation (7) and approximated by

$$\frac{d_1}{h} \approx \frac{\theta_{1B} - \bar{\theta}}{(\theta_{1B} - \bar{\theta}) - (\theta_{1T} - \bar{\theta})} \tag{32}$$

where the subscript 1 denotes the quantities at the midspan. Evidently, equations (31) and (32) suggest that the value of d_1/h would reach a plateau (constant) as $\bar{\theta}$ is large. In fact, this is indeed the case in Fig. 9. For the case of $\bar{k} = 1.0$, the d_1/h curve reaches a plateau of value 0.51 for $\bar{\theta}$ approximately equal to 1.75%. It is expected that the other two curves would also behave in a similar manner and find their own plateaus as $\bar{\theta}$ becomes large.

The bending moment at the end of the specimen may be found from

$$M = P(\delta^* - L\alpha) \tag{33}$$

This equation was derived in Ref. [3] and is shown in Fig. 3. The moment M is plotted in Fig. 10 for the three cases considered. It is found that the load P and the distance d_s affect the end moment greatly. As far as the strain rate effect is concerned, the magnitude of the end moment is greater at greater strain rate. This is resulted from the larger stress that a specimen can sustain at a higher strain rate for a fixed plastic strain. Hence, the load P is also greater for greater strain rate. On the other hand, due to the influence of d_s, the end moment follows the trend of d_s and reaches a maximum value at the small strain range and then drops off rapidly and approaches a plateau at large strain.

The deflection curves are shown in Fig. 11 for three levels of $\bar{\theta}$ for $\bar{k}$ = 1 and two levels each for $\bar{k}$ = 0.75 and 0.60. Within the range of investigation, it is found that the rate of deflection decreases as the plastic strain increases.

Finally, the solutions presented above are compared with those obtained from a more restricted formulation given in Appendix A, in which the strain rate is assumed to be uniform throughout the specimen. Figures 12-14 show the results from both formulations for the case of $\bar{k}$ = 1.0. With respect to the solutions of the nonuniform strain rate formulation, the predicted misalignment errors and the shifting of the N.A. by the uniform strain rate formulation are overestimated at the small strain range and underestimated at the larger strain range. For the uniform strain rate formulation, the function k is uniform across the cross-section and the N.A. returns to the geometric centerline of the specimen at large strain. Although strain rate was not considered a factor in the work of Wu and Rummeler [3], it is seen that the formulation of [3] belongs to that of the uniform strain rate formulation and the N.A. would also return to the geometric centerline at larger strain level.

The above two formulations are correlated during the course of numerical calculation. The results of the uniform strain rate formulation serve as the initial guess for the solution of the highly nonlinear equations obtained from the nonuniform strain rate formulation. The procedures of computation are presented in Appendix B. Since only the monotonic loading condition is of interest here, the step size $\Delta\bar{\theta}$ is assigned for each iteration. It is found that for the purpose of rapid convergence, $\Delta\bar{\theta}$ should increase with the plastic strain. However, due to the small number of elements used in the discrete model, the numerical results at larger strain level are unstable at the grip ends of the specimen (but is stable elsewhere in the specimen). It takes a great amount of trial and error procedure to select a correct step size so that the numerical output is convergent. It is anticipated that the problem of numerical instability mentioned above would be improved with greater number of elements taken in the discretized model.

5. CONCLUSIONS

The following conclusions may be drawn from the present study of 1100-0 aluminum specimens:

(1) Based on the endochronic constitutive equation, the formulation of the misalignment problem in the dynamic tension test has been developed. Two assumptions are made: (a) plane cross-sections remain plane during deformation; and (b) the strain rate history effect is negligible in the computation of stress (equation (8)). The second assumption is justifiable due to the extremely small variation in the strain rate throughout the tension test for each element of the discrete model.

(2) The lower the strain rate is at the tension test, the more significant the misalignment errors become. Three levels of strain rate, i.e., 1.30×10^{-5}, 1.24×10^{-2}, and 7.63×10^{-1} sec^{-1} are investigated. In this strain rate range, the misalignment error at the geometrical centerline of the specimen is within 2% and vanishes mostly as the plastic strain increases beyond 2%. At the extreme fibers of the specimen, the misalignment errors approach to 50% at the very small plastic strain range. Therefore, any investigation related to the local deformation of the extreme fibers will have to account for the misalignment effect.

(3) In the range of plastic deformation, the error introduced by misalignment decreases with the magnitude of plastic strain. Hence, it is conjectured that the most significant effect of misalignment occurs at the interface between the elastic and the plastic range. This conjecture is in agreement with the finding of Wu and Rummler [3] that the most significant error occurs at the knee portion of the stress-strain curve.

(4) At the midspan of the specimen, the variation of strain rate between extreme fibers decreases with increasing plastic strain. The strain rate reaches a uniform value at plastic strain equal to 0.8%.

(5) The N.A. will shift toward the geometrical centerline of the specimen as the plastic strain increases. But, it will reach a limit and will not move back to the geometrical centerline at large plastic strain as anticipated by the uniform strain rate formulation.

(6) The misalignment errors and the shifting of the N.A. predicted by the uniform strain rate formulation in which the strain rate is constant for the whole specimen are always overestimated at the small plastic strain range and underestimated at the larger plastic strain range.

(7) The formulation of Wu and Rummler [3] belong to the case of uniform strain rate formulation.

6. ACKNOWLEDGEMENT

The authors wish to express their sincere thanks to Dr. D.R. Rummler of NASA-Langley Research Center for providing the NONLIN subroutine which was instrumental in obtaining the numerical solutions reported herein. This research was supported by NASA Grant No. NSG 1499 through Langley Research Center.

RERERENCES

1. Penny, R. K., and Leckie, F. A., "The Mechanics of Tensile Testing," International Journal of Mechanical Science, Vol. 10, 1968, pp. 262-273.
2. Christ, B. W., and Swanson, S. R., "Alignment Problems in the Tensile Test," Journal of Testing and Evaluation, Vol. 4, 1976, pp. 405-417.
3. Wu, H. C., and Rummler, D. R., "Analysis of Misalignment in the Tension Test," ASME Journal of Engineering Materials and Technology, Vol. 101, 1979, pp. 68-74.
4. Wu, H. C., and Chen, L., "Endochronic Theory of Transient Creep and Creep Recovery," Report G302-79-001, Division of Material Engineering, The University of Iowa, April 1979.
5. Wu, H. C., and Yip M. C., "Strain Rate and Strain Rate History Effects on the Dynamic Behavior of Metallic Materials," International Journal of Solids and Structures, 1980 (in press).
6. Valanis, K. C., "Fundamental Consequences of a New Intrinsic Time Measure - Plasticity as a Limit of the Endochronic Theory," Report G224-DME-78-001, Division of Materials Engineering, The University of Iowa, 1978.

FIGURE CAPTIONS

Fig. 1 Strain Rate Sensitivity Function for 1100-0 Al

Fig. 2 Constant Strain Rate Stress-Strain Curves

Fig. 3 (a) Specimen Dimensions and the Coordinate System,
(b) The Load Train Configuration of the Symmetric Case of Misalignment

Fig. 4 The Discrete Numerical Model

Fig. 5 The Normalized Strain Rate Sensitivity Function of Top and Bottom Fibers at Midspan

Fig. 6 Variation of k at the Midspan with Respect to the Width of the Specimen

Fig. 7 Center Error at the Midspan

Fig. 8 Misalignment Errors of the Top and Bottom Fibers at the Midspan

Fig. 9 Location of N.A. at the Midspan

Fig. 10 The End Moment

Fig. 11 The Deflection Curves

Fig. 12 Center Error for the Two Formulations ($\bar{k} = 1.0$)

Fig. 13 Errors at Bottom and Top Fibers for the Two Formulations ($\bar{k} = 1.0$)

Fig. 14 Locaton of N.A. for the Two Formulations ($\bar{k} = 1.0$)

APPENDIX A - Uniform Strain Rate Formulation

In this formulation, the strain rate is assumed to be constant throughout the specimen in addition to the usual assumption that plane cross-sections remain plane during deformation. The load and moment balance equations are obtained in closed form. Thus, in order to obtain a numerical solution, it is only necessary to cut the specimen into I element along the x-direction.

Balance of force gives

$$P = \int_A \sigma \, dA = b\rho \int_{\zeta_T}^{\zeta_B} \sigma \frac{d\varepsilon}{d\zeta} \, d\zeta \tag{A1}$$

where subscripts T and B indicate location at top and bottom fibers, respectively. Since, for monotonic loading,

$$d\zeta = k(\dot{\theta}) d\theta = k(\dot{\theta}) \left(d\varepsilon - \frac{d\sigma}{E} \right) \tag{A2}$$

it follows

$$\frac{d\varepsilon}{d\zeta} = \frac{1}{k(\dot{\theta})} + \frac{1}{E} \frac{d\sigma}{d\zeta} \tag{A3}$$

Note that in this formulation $k(\dot{\theta})$ is constant throughout the test.

Equations (1), (A1), and (A3) combine to give

$$P = \frac{b\rho}{k^2} \left\{ \left(\frac{\sigma_0}{2\beta} + \frac{\sigma_0^2}{2E} \right) \bar{z}^2 + (\sigma_0 - \sigma_y) \left[\frac{1}{(n-2)\beta} - \frac{\sigma_0}{E} \right] \bar{z}^{-n+2} \right.$$

$$\left. + \frac{1}{2E} (\sigma_0 - \sigma_y)^2 \, \bar{z}^{-2n+2} \right\}_{\bar{z}_T}^{\bar{z}_B} , \quad \text{for } \zeta > 0 \tag{A4}$$

where $\bar{z} = 1 + \beta\zeta$.

The balance of moment is

$$M(x) = -\int_A \sigma y \, dA = -\rho \, \bar{\varepsilon} A + b\rho^2 \int_{\varepsilon_T}^{\varepsilon_B} \sigma\varepsilon \, d\varepsilon \tag{A5}$$

which may be written as

$$M(x) = -\rho\bar{\varepsilon} P + b\rho^2(M_1 + M_2 + M_3 + M_4) \tag{A6}$$

where

$$M_1 = \int_{\zeta_T}^{\zeta_B} \frac{\sigma\zeta}{k^2} \, d\zeta$$

$$= \frac{1}{\beta^2 k^3} \left[-\frac{\sigma_0^2}{2} \bar{z}^2 + \frac{\sigma_0}{3} \bar{z}^3 - \left(\frac{\sigma_0 - \sigma_y}{3 - n}\right) \bar{z}^{-n+3} + \left(\frac{\sigma_0 - \sigma_y}{2 - n}\right) \bar{z}^{-n+2} \right]_{\bar{z}_T}^{\bar{z}_B} \tag{A7}$$

$$M_2 = \int_{\zeta_T}^{\zeta_B} \frac{\sigma^2}{kE} \, d\zeta$$

$$= \frac{1}{k^3 E\beta} \left[\frac{\sigma_0^2}{3} \bar{z}^3 + \frac{(\sigma_0 - \sigma_y)^2}{3 - 2n} \bar{z}^{-2n+3} - \frac{2\sigma_0(\sigma_0 - \sigma_y)}{3 - n} \bar{z}^{-n+3} \right]_{\bar{z}_T}^{\bar{z}_B} \tag{A8}$$

$$M_3 = \int_{\zeta_T}^{\zeta_B} \frac{\sigma\zeta}{kE} \frac{d\sigma}{d\zeta}$$

$$= \frac{1}{k^3 E\beta} \left[-\frac{\sigma_0^2}{2} \bar{z}^2 + \frac{\sigma_0^2}{3} \bar{z}^3 - (2 - n)\sigma_0(\sigma_0 - \sigma_y) \frac{\bar{z}^{-n+3}}{3 - n} \right. \tag{A9}$$

$$\left. + \sigma_0(\sigma_0 - \sigma_y)\bar{z}^{-n+2} + (1 - n)(\sigma_0 - \sigma_y) \frac{\bar{z}^{-2n+3}}{3 - 2n} - (\sigma_0 - \sigma_y)^2 \frac{\bar{z}^{-2n+2}}{2} \right]_{\bar{z}_T}^{\bar{z}_B}$$

and

$$M_4 = \int_{\zeta_T}^{\zeta_B} \frac{\sigma^2}{r^2} \frac{d\sigma}{d\zeta} d\zeta$$

$$= \frac{1}{E^2 k^3} \left[\frac{\sigma_0^3}{3} \bar{z}^3 - \sigma_0^2(\sigma_0 - \sigma_y)\bar{z}^{-n+3} + \sigma_0(\sigma_0 - \sigma_y)^2 \bar{z}^{-2n+3} \right.$$

$$\left. - (\sigma_0 - \sigma_y)^3 \frac{\bar{z}^{-3n+3}}{3} \right]_{\bar{z}_T}^{\bar{z}_B} \tag{A10}$$

To arrive at the above equations, equation (A2) was integrated with the requirement of monotonic loading beginning at the zero stress state. Thus,

$$\varepsilon = \frac{\zeta}{k} + \frac{\sigma}{E} \tag{A11}$$

Combining equations (A11) and (1), the following relation is obtained

$$1 + \beta k \varepsilon = \left(1 + \frac{\beta \sigma_0}{E}\right) \bar{z} - \frac{\beta}{E} (\sigma_0 - \sigma_y)\bar{z}^{-n+1} \tag{A12}$$

Hence, the variables u, ρ, ε_T, ε_B, $\bar{z}_T$ and $\bar{z}_B$ can be solved numerically from the system of equations (A4), (A6), (A12), (6), (22) and (25) subjected to the boundary conditions given by equations (27) and (28).

APPENDIX B - Numerical Procedures for the Nonuniform Strain Rate Formulation

In this calculation, the specimen is discretized into 4 elements along both the longitudinal (I = 4) and the lateral (J = 4) directions. Algebraically, there are 55 unknown variables with 55 nonlinear equations. They are:

Variables: σ_{ij} (20), ε_{iT} (5), ε_{iB}(5), ζ_{ij} (20), u_i(4), d_s(1)

Equations: eq. (8) - 20, eq. (15) - 20, eq. (18) - 5, eq. (21) - 5, eq. (24) - 1, eq. (27) - 4.

The computation of k_{ij} needs special attention. Specifically, the following expression should be incorporated into equation (10):

$$\ell n \left(\frac{\dot{\theta}_{ij}}{\dot{\bar{\theta}}}\right) = \ell n \left(\frac{\dot{\varepsilon}_{ij} - \dot{\sigma}_{ij}/E}{\dot{\bar{\varepsilon}} - \dot{\bar{\sigma}}/E}\right) = \ell n \left(\frac{\Delta\varepsilon_{ij} - \Delta\sigma_{ij}/E}{\Delta\bar{\varepsilon} - \Delta\bar{\sigma}/E}\right)$$

$$= \ell n \left\{\frac{(\varepsilon_{ij}^{(n)} - \varepsilon_{ij}^{(n-1)}) - (\sigma_{ij}^{(n)} - \sigma_{ij}^{(n-1)})/E}{(\bar{\varepsilon}^{(n)} - \bar{\varepsilon}^{(n-1)}) - (\bar{\sigma}^{(n)} - \bar{\sigma}^{(n-1)})/E}\right\} \qquad \text{(B1)}$$

where $\varepsilon_{ij}^{(n)}$ is the strain at the nth step and $\varepsilon_{ij}^{(n-1)}$ is that of the previous step.

The numerical procedures are as follows:

1. Use the solution of the uniform strain rate formulation as the initial guess to compute the first solution of the nonuniform formulation. This solution is the first loading step beyond the elastic limit. In obtaining this solution, the yield stress σ_{ij}^{Y} and the yield strain ε_{ij}^{Y} are used as the corresponding values for the $(n-1)^{th}$ step. In this case, equation (B1) is reduced to

$$\ell n\left(\frac{\dot{\theta}_{ij}}{\dot{\bar{\theta}}}\right) = \ell n\left(\frac{\varepsilon_{ij} - \sigma_{ij}/E}{\bar{\varepsilon} - \bar{\sigma}/E}\right) \qquad \text{(B2)}$$

2. Increase $\bar{\zeta}$ or $\bar{\theta}$ by a prescribed step size $\Delta\bar{\zeta}$ or $\Delta\bar{\theta}$.

3. Calculate the mean stress, mean strain and load for the new step.

4. Modify the true solution of the previous step according to the ratio $\bar{\zeta}^{(n)}/\bar{\zeta}^{(n-1)}$ and input the modified results as the initial guess for the current step of computation.

5. Solve the system of equations and calculate the misalignment errors. Note that in this step, the expression (B1) should be used.

6. Repeat Steps 2 through 5. The computation terminates at a prescribed strain. Note that the step size $\Delta\bar{\theta}$ needs to be increased with θ.

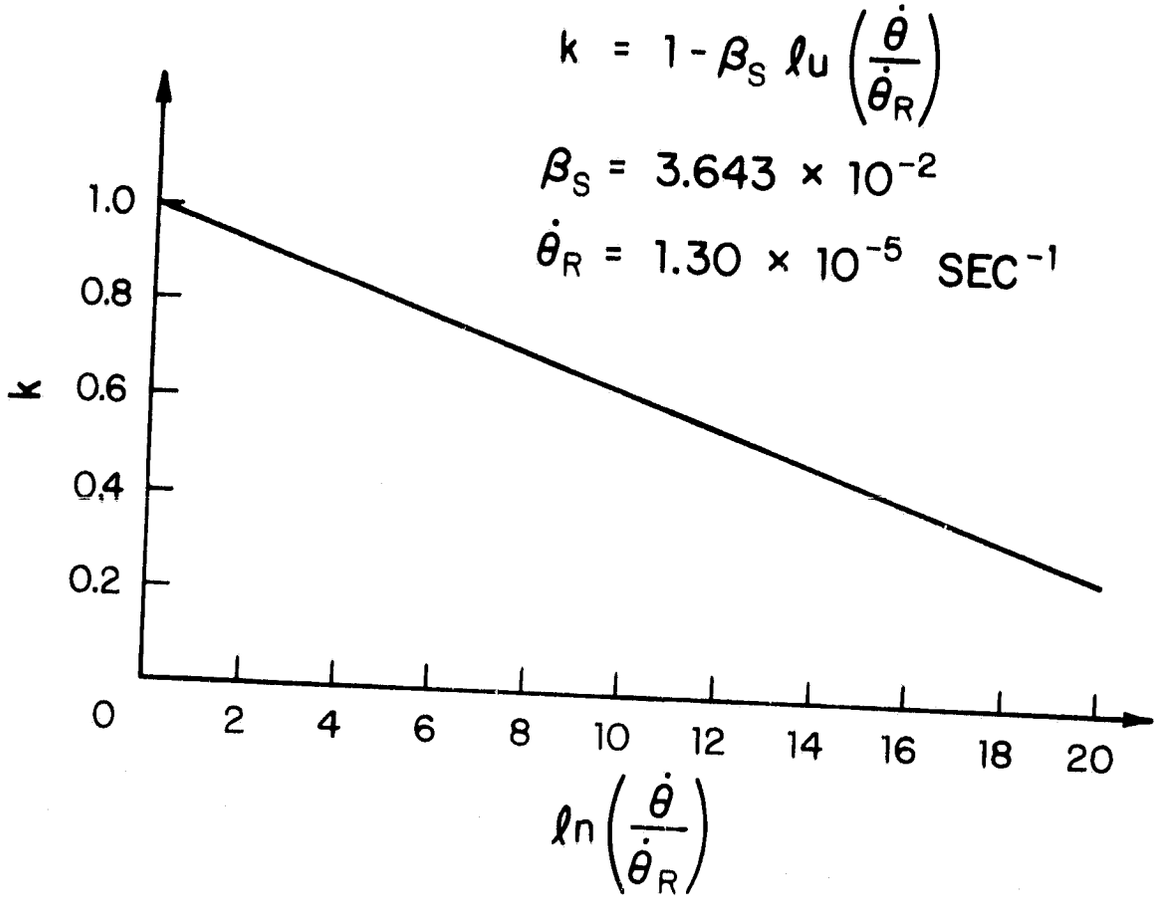
$k = 1 - \beta_S \ell u \left(\frac{\dot{\theta}}{\dot{\theta}_R}\right)$
$\beta_S = 3.643 \times 10^{-2}$
$\dot{\theta}_R = 1.30 \times 10^{-5}$ SEC^{-1}
k
1.0
0.8
0.6
0.4
0.2
0
2
4
6
8
10
12
14
16
18
20
$\ell n \left(\frac{\dot{\theta}}{\dot{\theta}_R}\right)$

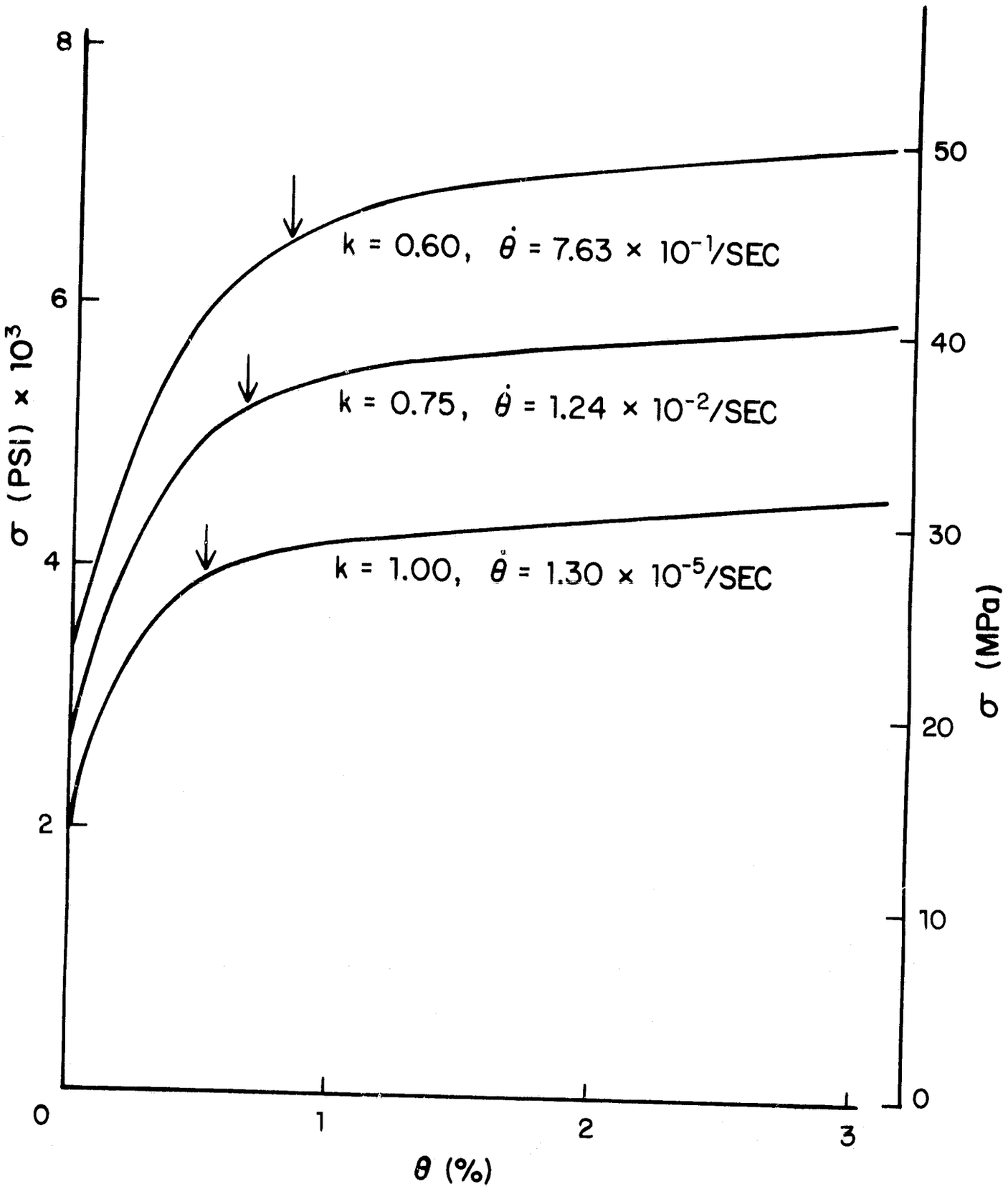
8
6
4
2
0
σ (PSI) x 10³
50
40
30
20
10
0
σ (MPa)
k = 0.60, θ̇ = 7.63 x 10⁻¹/SEC
k = 0.75, θ̇ = 1.24 x 10⁻²/SEC
k = 1.00, θ̇ = 1.30 x 10⁻⁵/SEC
0
1
2
3
θ (%)

(a)

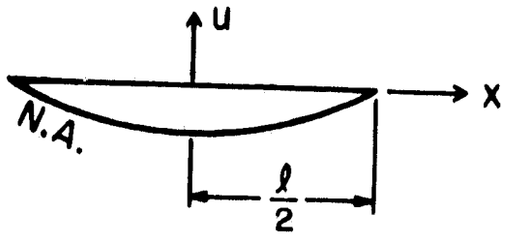

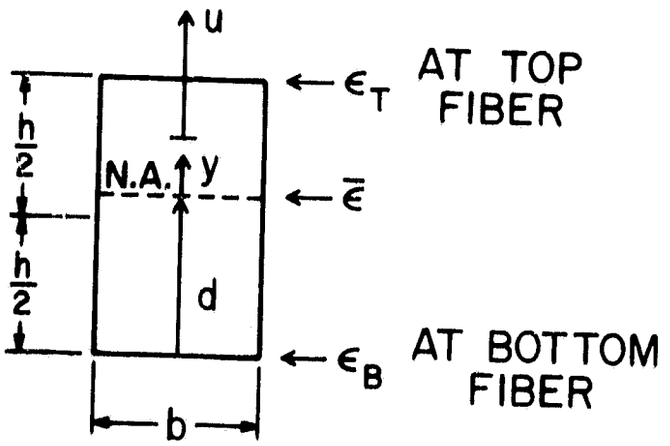

(b)

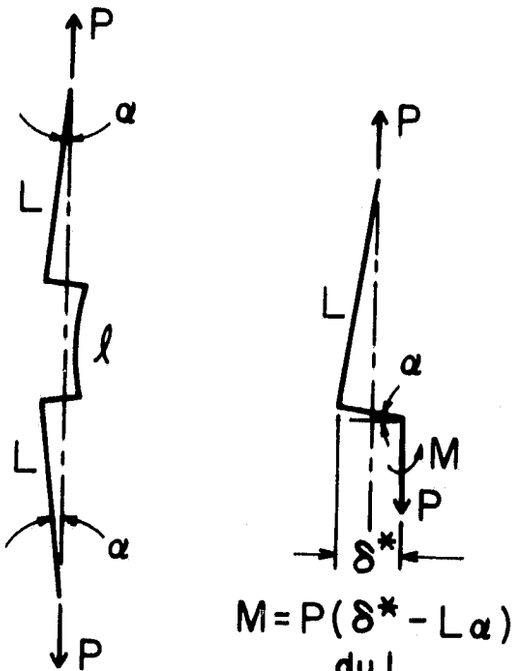

$$M = P(\delta^* - L\alpha)$$

$$\alpha = \left.\frac{du}{dx}\right|_{x=\frac{\ell}{2}}$$

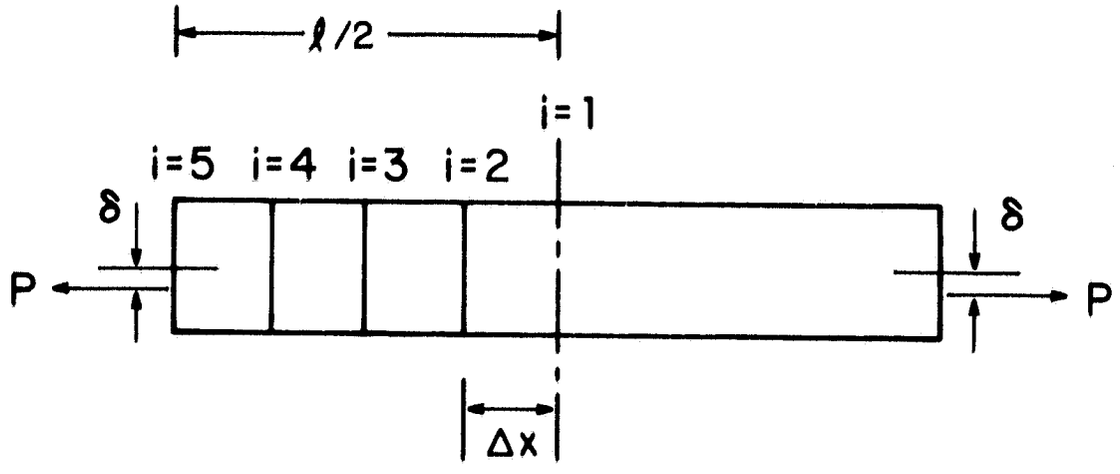

(a)

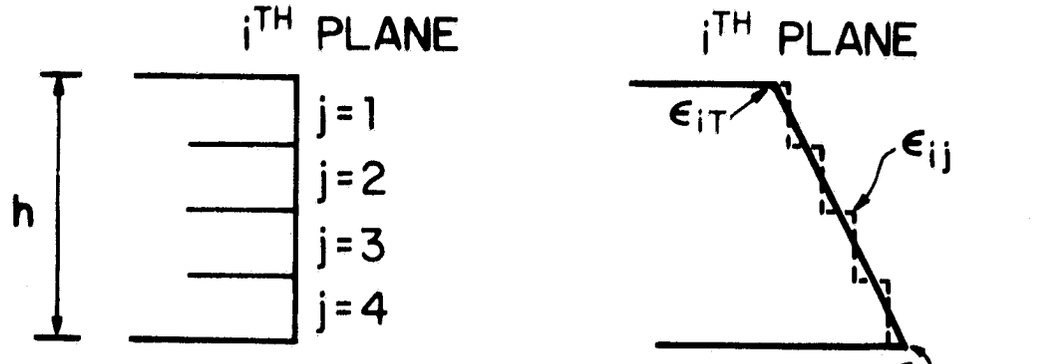

(b)

--- DISCRETIZED STRAIN

— ACTUAL STRAIN IN THE i^{TH} PLANE

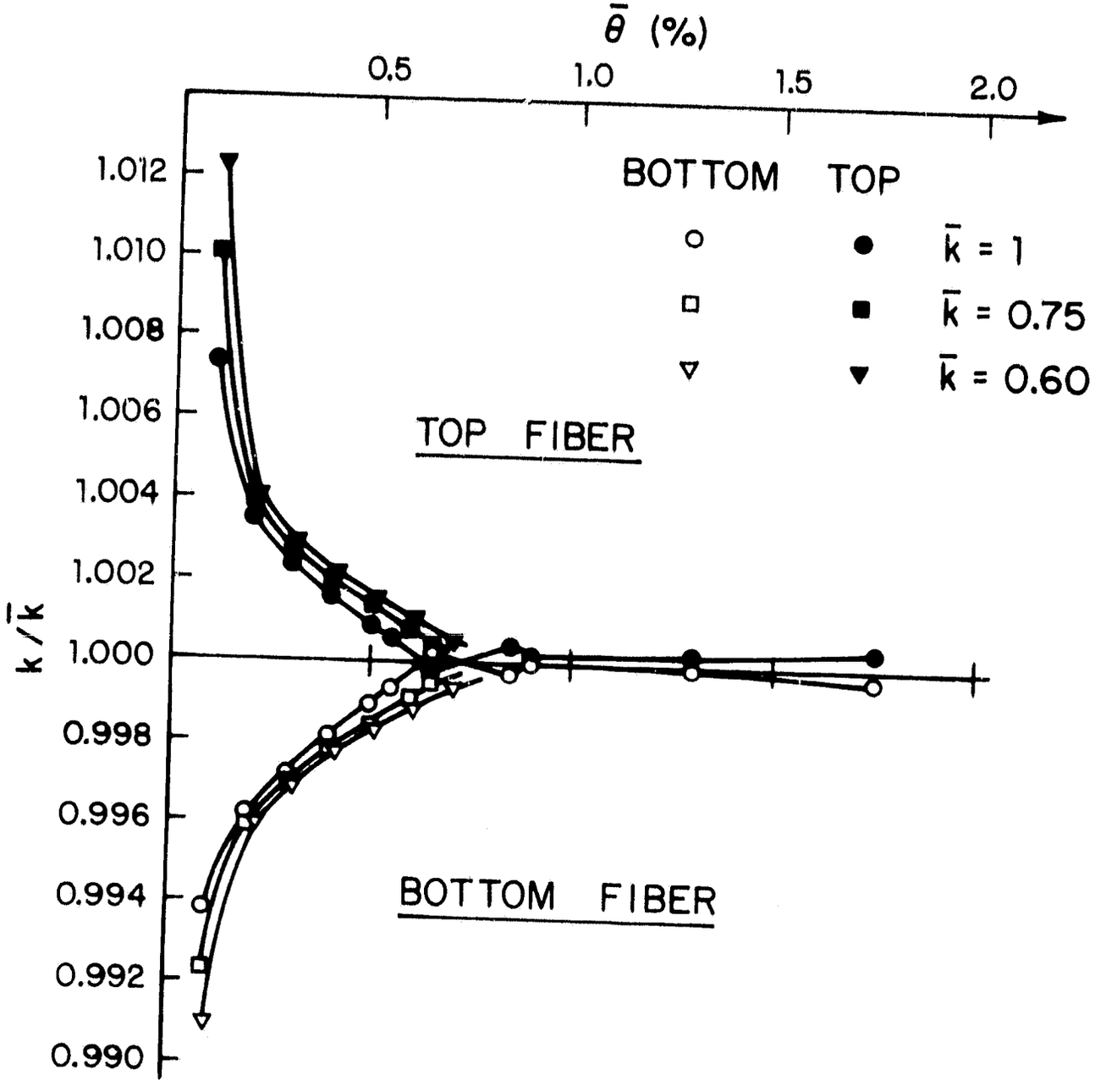
$\bar{\theta}$ (%)
0.5
1.0
1.5
2.0
BOTTOM TOP
$\bar{k}$ = 1
$\bar{k}$ = 0.75
$\bar{k}$ = 0.60
TOP FIBER
BOTTOM FIBER
k/$\bar{k}$
1.012
1.010
1.008
1.006
1.004
1.002
1.000
0.998
0.996
0.994
0.992
0.990

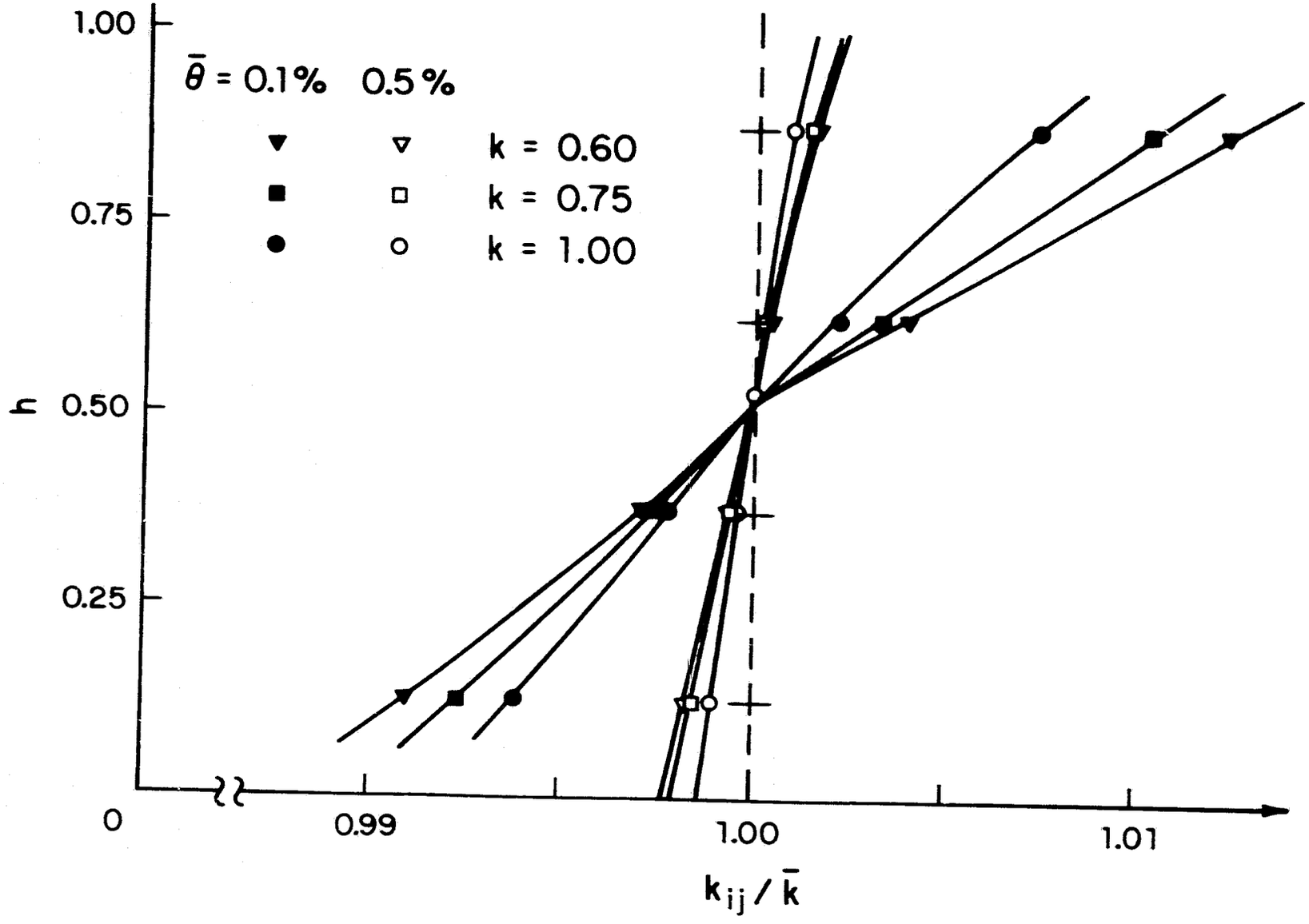
1.00
0.75
0.50
0.25
0
$\bar{\theta}$ = 0.1% 0.5%
k = 0.60
k = 0.75
k = 1.00
f
0.99
1.00
1.01
$k_{ij} / \bar{k}$

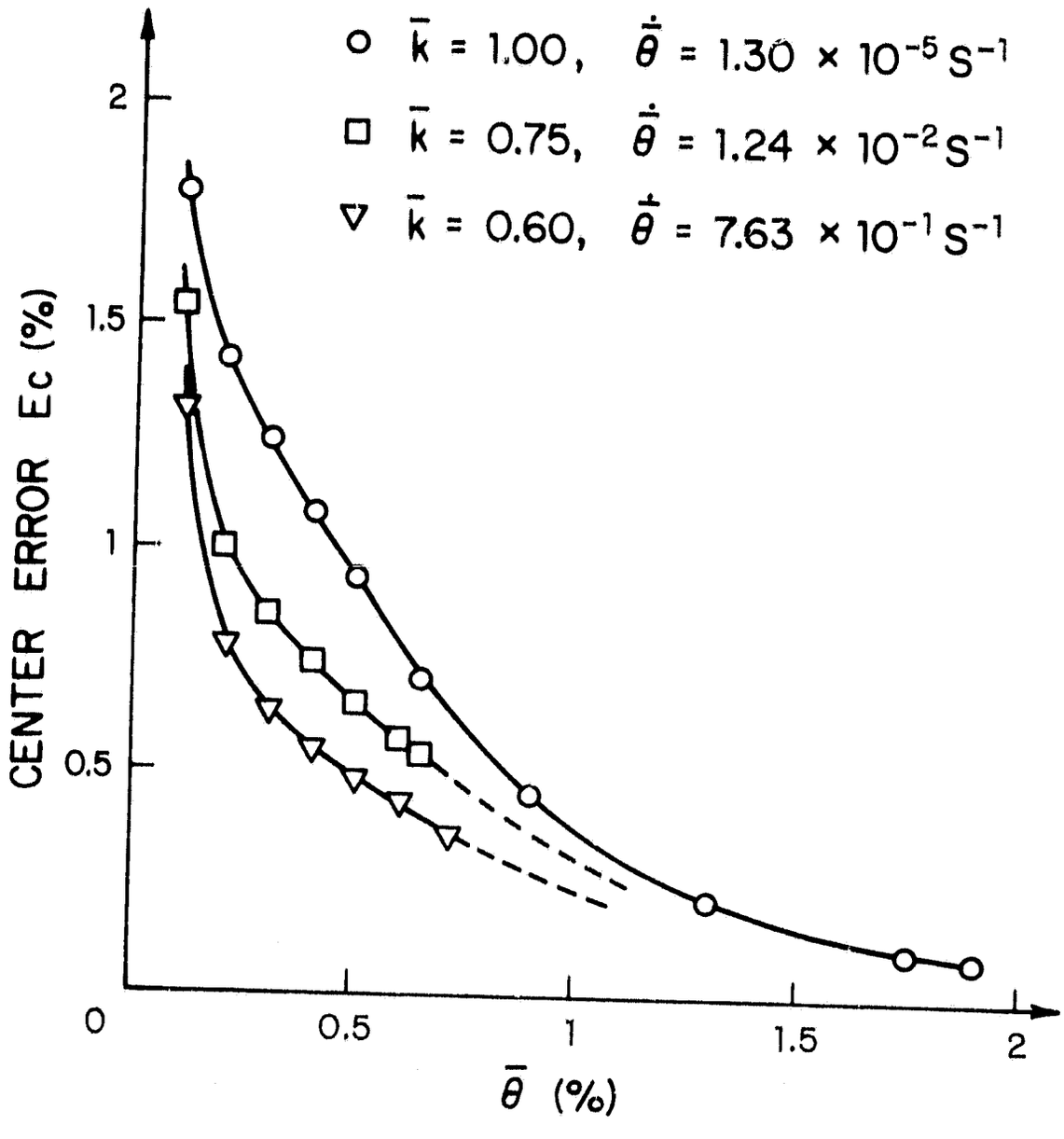
○ $\bar{k}$ = 1.00, $\dot{\bar{\theta}}$ = 1.30 × 10⁻⁵ S⁻¹
□ $\bar{k}$ = 0.75, $\dot{\bar{\theta}}$ = 1.24 × 10⁻² S⁻¹
▽ $\bar{k}$ = 0.60, $\dot{\bar{\theta}}$ = 7.63 × 10⁻¹ S⁻¹
CENTER ERROR Ec (%)
2
1.5
1
0.5
0
0.5
1
1.5
2
$\bar{\theta}$ (%)

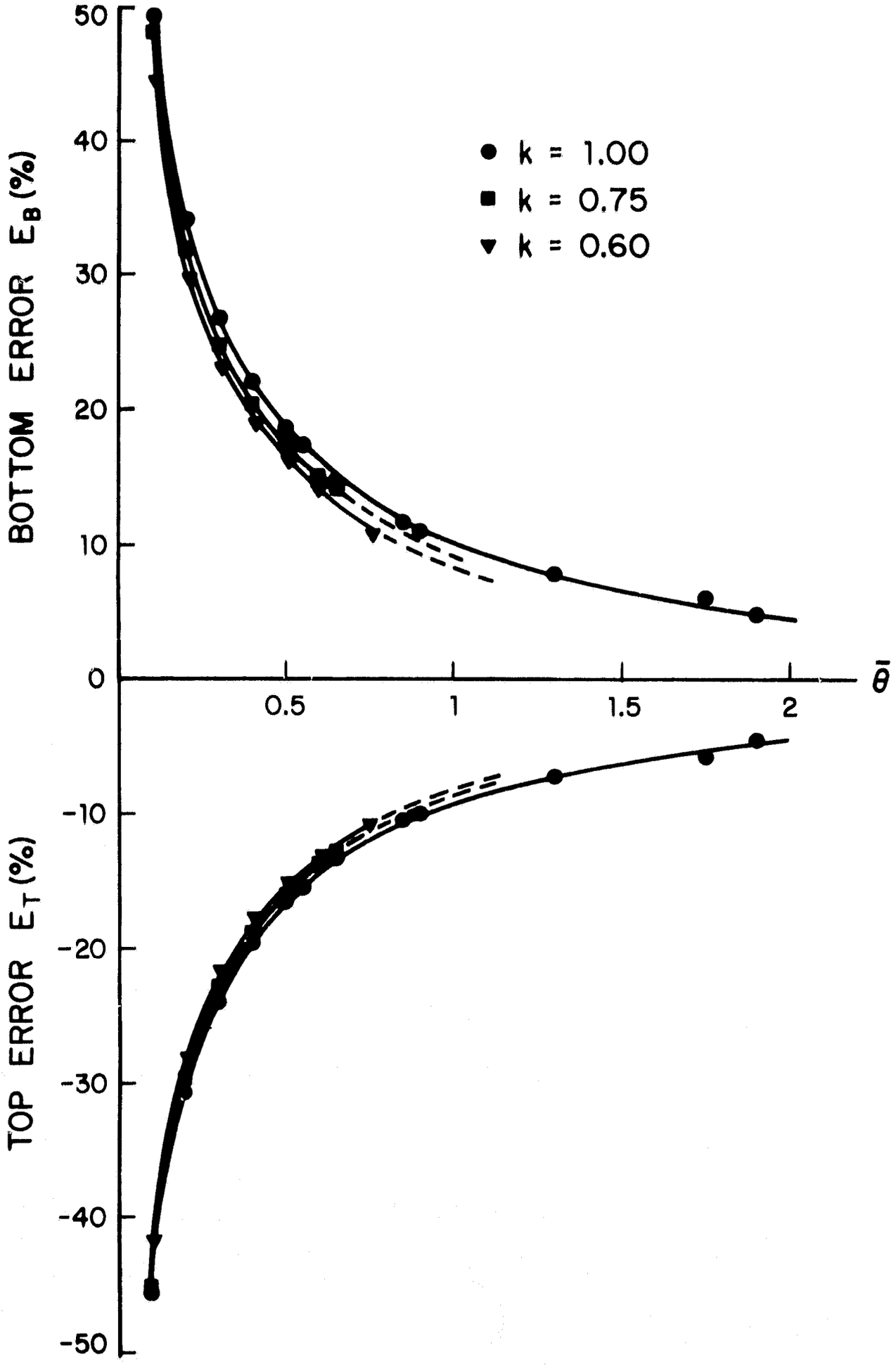
50
40
30
20
10
0
-10
-20
-30
-40
-50
0.5
1
1.5
2
$\bar{\theta}$
BOTTOM ERROR E_B (%)
TOP ERROR E_T (%)
k = 1.00
k = 0.75
k = 0.60

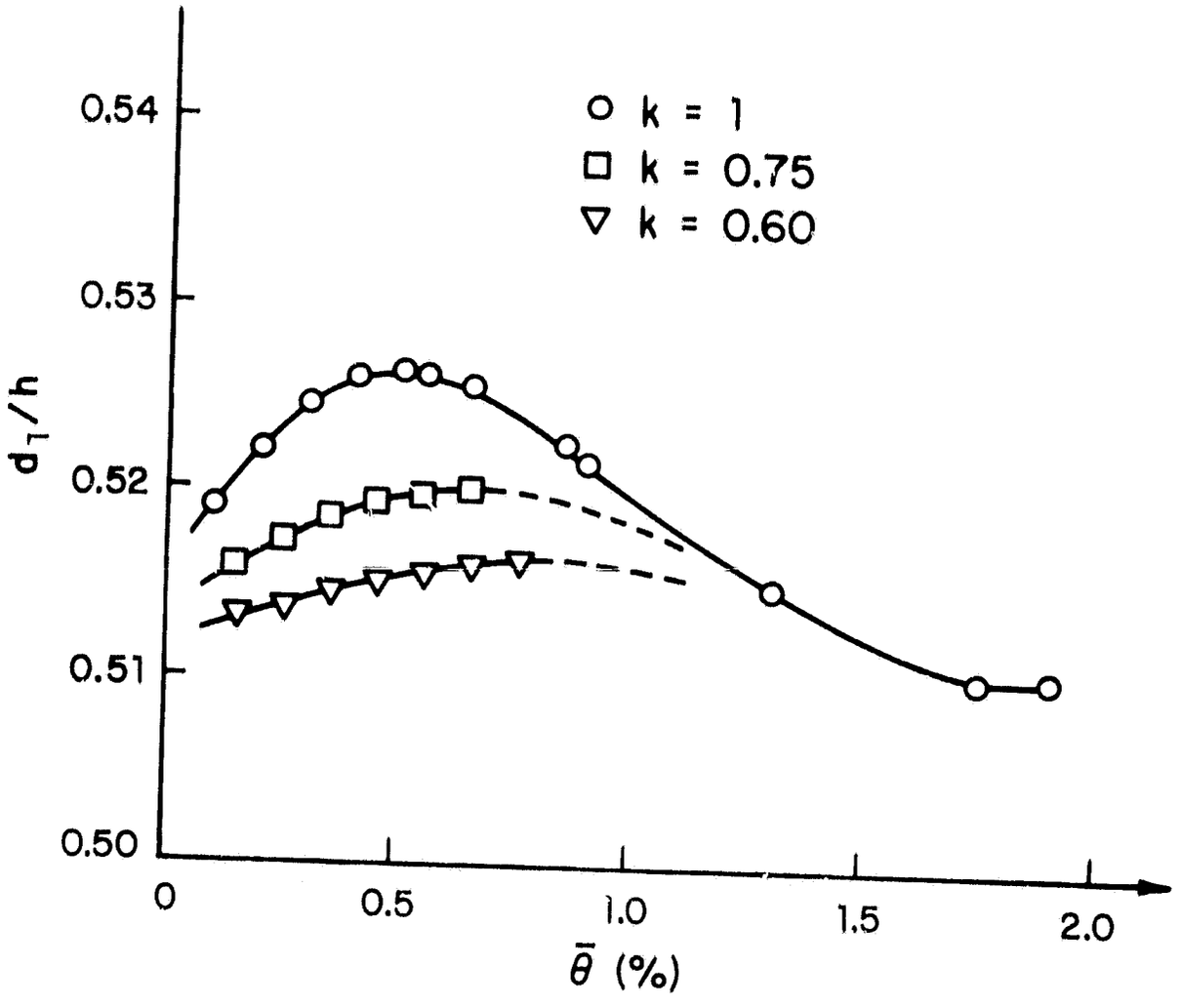
0.54
0.53
0.52
0.51
0.50
d_1/h
k = 1
k = 0.75
k = 0.60
0
0.5
1.0
1.5
2.0
$\bar{\theta}$ (%)

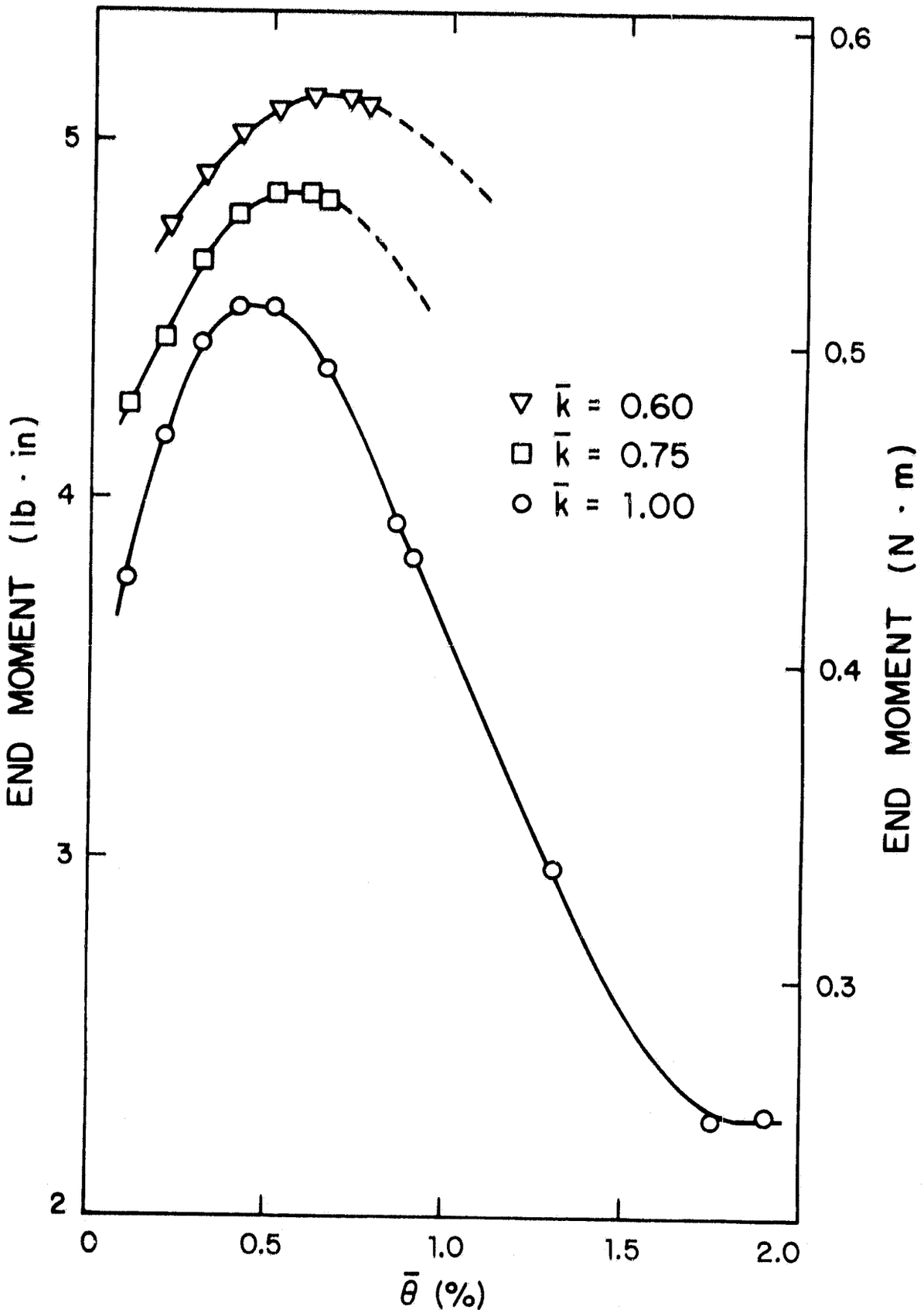
END MOMENT (lb · in)
END MOMENT (N · m)
$\bar{\theta}$ (%)
$\bar{k}$ = 0.60
$\bar{k}$ = 0.75
$\bar{k}$ = 1.00
5
4
3
2
0.6
0.5
0.4
0.3
0
0.5
1.0
1.5
2.0

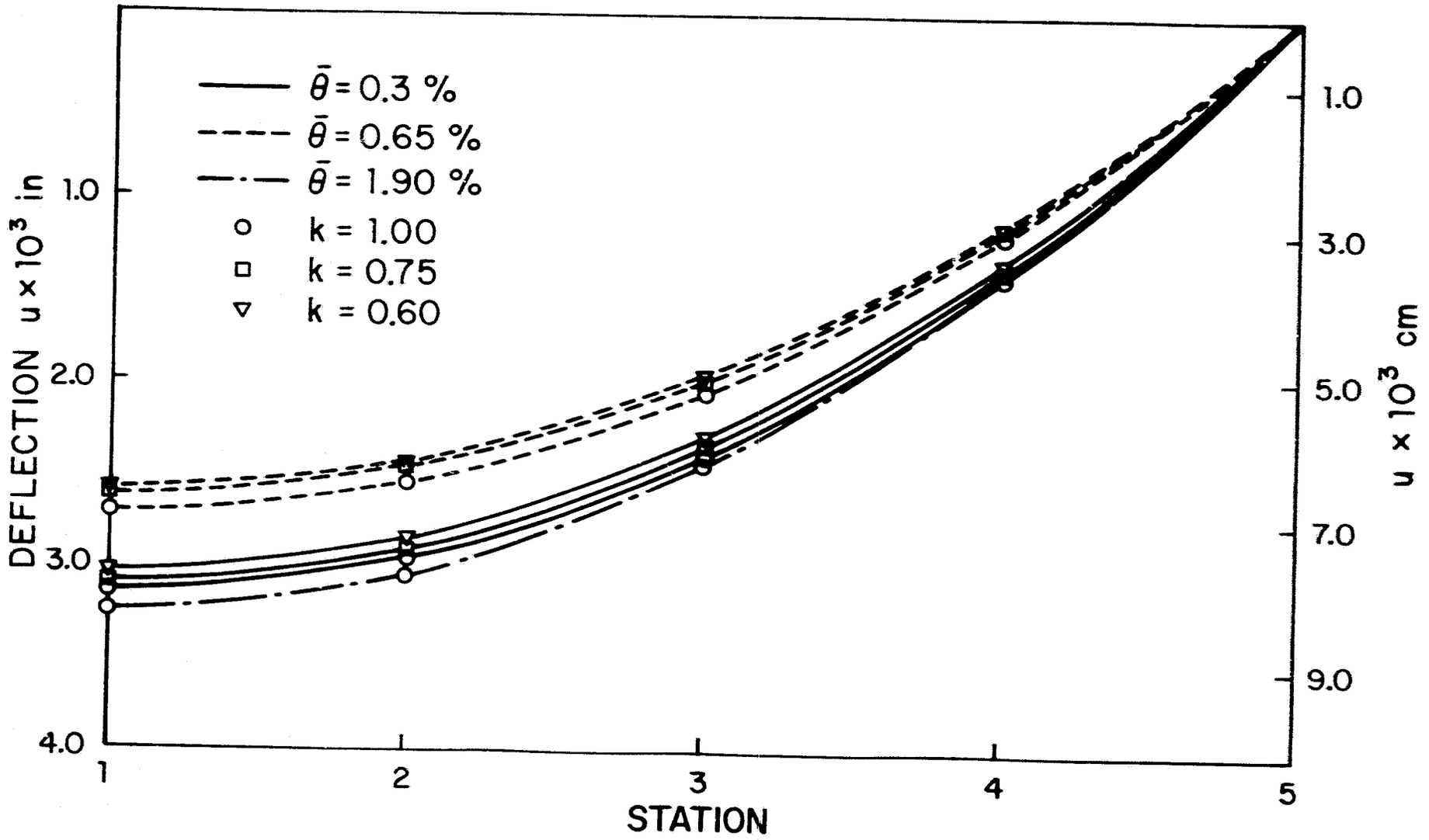
$\bar{\theta}$ = 0.3 %
$\bar{\theta}$ = 0.65 %
$\bar{\theta}$ = 1.90 %
k = 1.00
k = 0.75
k = 0.60
DEFLECTION u x 10³ in
1.0
2.0
3.0
4.0
1.0
3.0
5.0
7.0
9.0
u x 10³ cm
1
2
3
4
5
STATION

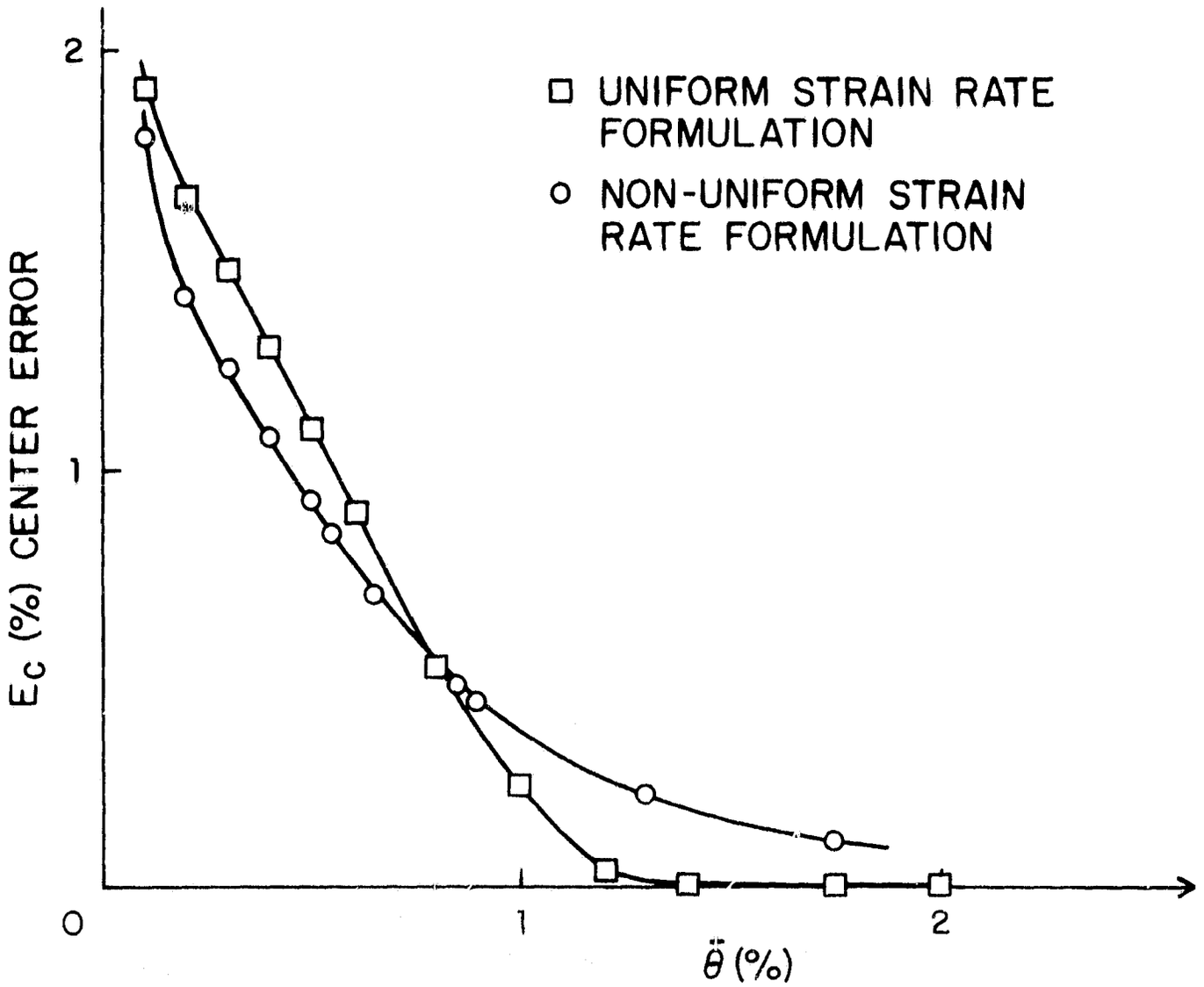
UNIFORM STRAIN RATE FORMULATION
NON-UNIFORM STRAIN RATE FORMULATION
E_C (%) CENTER ERROR
2
1
0
1
2
$\ddot{\theta}$ (%)

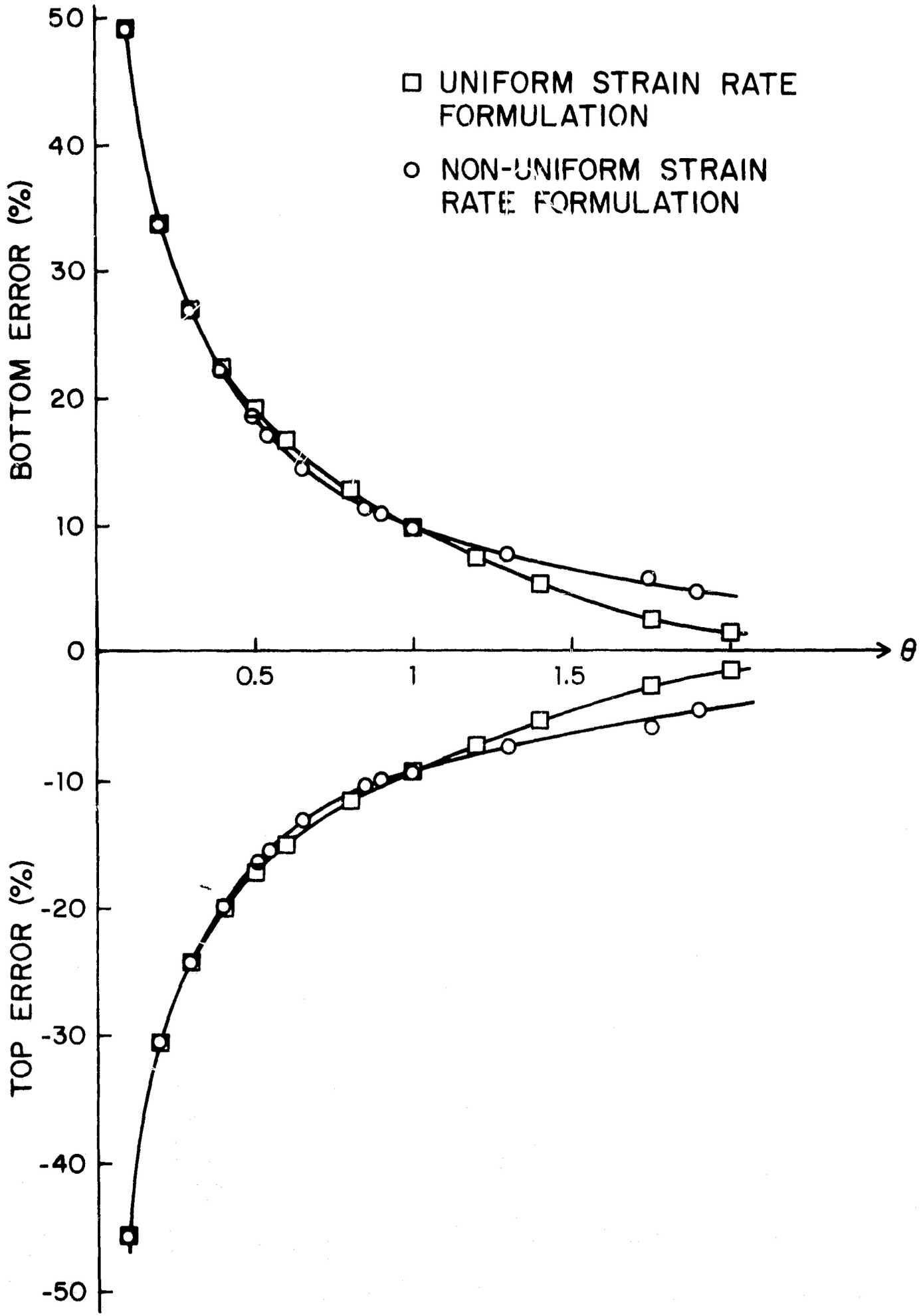
50
40
30
20
10
0
-10
-20
-30
-40
-50
BOTTOM ERROR (%)
TOP ERROR (%)
0.5
1
1.5
θ
UNIFORM STRAIN RATE FORMULATION
NON-UNIFORM STRAIN RATE FORMULATION

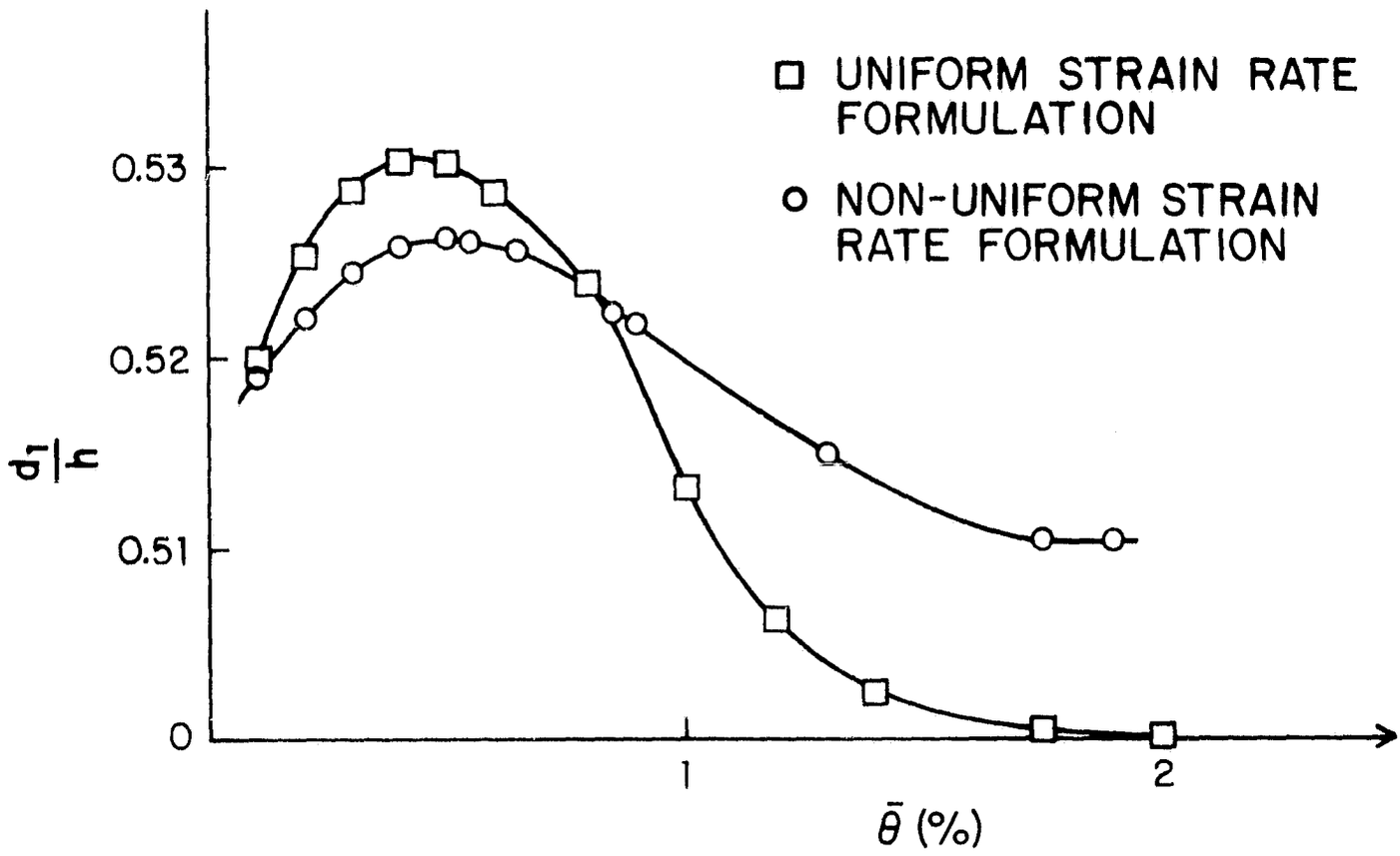
UNIFORM STRAIN RATE FORMULATION
NON-UNIFORM STRAIN RATE FORMULATION
0.53
0.52
0.51
0
1
2
σ_1/μ
$\bar{\theta}$ (%)